RSC Medicinal Chemistry

ROYAL SOCIETY OF CHEMISTRY

RESEARCH ARTICLE

Cite this: *RSC Med. Chem.*, 2025, **16**, 2743

The development of a PET radiotracer for imaging alpha synuclein aggregates in Parkinson's disease†

Gui-Long Tian,[a] Chia-Ju Hsieh,[a] Dinahlee Saturnino Guarino,[a] Thomas J. A. Graham,[a] Zsofia Lengyel-Zhand,[a] Alexander Schmitz,[a] Wai Kit Chia,[a] Anthony J. Young,[a] John-Grey Crosby,[a] Konstantinos Plakas,[a] Tianyu Huang,[b] Hao Jiang,[b] Yanbo Yu,[b] Catherine Hou,[a] Hsiaoju Lee,[a] E. James Petersson,[c] Sam Giannakoulias,[c] Jennifer O'Shea,[d] Paul Kotzbauer,[d] Zhude Tu,[b] Chester A. Mathis[e] and Robert H. Mach*[a]

M503-1619 was identified as a promising ligand for positron emission tomography (PET) imaging of α-synuclein (α-Syn) pathology in Parkinson's disease (PD). An exemplar for binding site 9 (residues GLY-86, ILE-88, PHE-94 and LYS-96) of α-Syn fibrils was generated. An *in silico* ultrahigh throughput screening campaign was conducted using a 42 million compound library. Secondary *in silico* methods followed by visual inspection were used to select 6 compounds as candidates for *in vitro* binding studies. **M503-1619** was found to have a high binding affinity (K_i = 6.5 nM *versus* the site 9 radioligand [^{3}H]BF-2846) to α-Syn fibrils and low affinity for beta amyloid (K_i = 390 nM *versus* [^{3}H]PiB) in competition binding assays. Saturation binding assays of **[^{3}H]M503-1619** in human tissues confirmed its high affinity to α-Syn (PD tissue, K_D = 2.5 nM; Alzheimer's disease tissue, K_D = 37 nM; progressive supranuclear palsy tissue, K_D = 55 nM). Autoradiography studies demonstrated a higher binding of this radioligand in PD brain sections than in multiple system atrophy brain sections. PET studies with **[^{11}C]M503-1619** showed high brain uptake and rapid washout (whole brain peak to 60 min ratio = 3.2) in non-human primates. The results of this study suggest that **[^{11}C]M503-1619** is a lead compound for radiotracer development imaging α-Syn with PET.

Received 20th January 2025,
Accepted 16th March 2025

DOI: 10.1039/d5md00057b

rsc.li/medchem

1. Introduction

Parkinson's disease (PD) is the second most common and the fastest-growing neurodegenerative disease.[1,2] Insoluble α-synuclein (α-Syn) aggregates are the histopathologic hallmark of the synucleinopathies that include both PD and multiple system atrophy (MSA).[3,4] The development of a positron emission tomography (PET) radiotracer for imaging α-Syn is important for early diagnosis, monitoring of disease progression, and evaluation of the efficacy of therapeutic interventions to reduce α-Syn burden. The success in the development of PET radiotracers for imaging beta amyloid (Aβ)[5,6] and tau[7] in Alzheimer's disease (AD) has highlighted the need for a PET radiotracer for imaging α-Syn in the synucleinopathies. However, the pathway for developing a PET radiotracer for imaging α-Syn has proven to be far more challenging than the development of PET radiotracers for Aβ and tau.

There are several obstacles that must be overcome in developing a PET radiotracer for α-Syn. First, the concentration of α-Syn aggregates within the brain is lower than that of Aβ or tau.[8–10] Consequently, a high affinity for α-Syn aggregates is required for a PET radiotracer to succeed in translational imaging studies. Also, since α-Syn coexist and colocalize with Aβ and tau,[8,9,11] a PET radiotracer for α-Syn must have a high binding selectivity for α-Syn over Aβ and tau.[12] Finally, α-Syn is located intracellularly, hence, a successful α-Syn PET radiotracer should not only cross the blood–brain barrier, but it must also cross the neuronal cell membrane. These obstacles, together with the additional properties, a PET radiotracer must possess for central nervous system (CNS) imaging studies, such as appropriate physicochemical properties (*e.g.*, molecular weight, topological polar surface area, Log *D*, *etc.*) and favorable peripheral metabolism leading to polar metabolites, present a steep challenge in developing an α-Syn PET radiotracer.

[a] *Department of Radiology, Perelman School of Medicine, University of Pennsylvania, Philadelphia, PA, USA. E-mail: rmach@pennmedicine.upenn.edu*
[b] *Department of Radiology, Washington University, School of Medicine, Saint Louis, MO, USA*
[c] *Department of Chemistry, University of Pennsylvania, Philadelphia, PA, USA*
[d] *Department of Neurology, Washington University School of Medicine, Saint Louis, MO, USA*
[e] *Department of Radiology, University of Pittsburgh, Pittsburgh, PA, USA*

† Electronic supplementary information (ESI) available. See DOI: https://doi.org/10.1039/d5md00057b

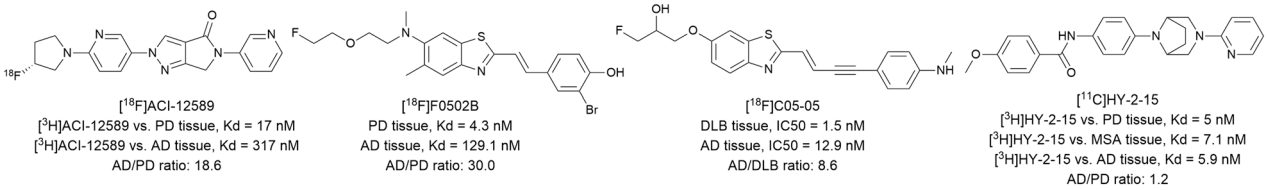

Fig. 1 Structure of recently developed α-Syn PET radiotracers.

In spite of the above limitations, there has been some recent success in the development of PET radiotracers for imaging α-Syn *in vivo* (Fig. 1). For example, [^{18}F]ACI-12589 is a PET radiotracer that has shown promise in imaging α-Syn in MSA but not PD patients.[13] In addition, Ye *et al.* have reported the radiotracer, [^{18}F]F0502B,[14] which is an analog of PBB3[15] (a mixed tau/α-Syn PET radiotracer) is capable of imaging α-Syn in autoradiography studies of PD brain. Although [^{18}F]F0502B is not a useful PET radiotracer for *in vivo* imaging studies, it is a good lead compound for further structure–activity relationship studies aimed at identifying a ligand having a better off-target binding profile and higher brain uptake. More recently, Endo *et al.* demonstrated that [^{18}F]C05-05 was able to image α-Syn in both PD and MSA patients.[16] However, the low brain uptake and high affinity of this radiotracer for tau limits its utility in PET imaging studies of α-Syn.

Based on the solid state nuclear magnetic resonance structure of α-Syn fibrils, our group identified multiple binding sites for small molecules in the "Greek key region" of the protein.[17] Using photo-crosslinking studies with mass spectrometry, we confirmed that there are two binding sites which can bind small molecules with nanomolar affinity, site 2 and site 9. "Site 2" is located towards the N-terminus of the Greek key motif and contains TYR-39, SER-42 and THR-44, whereas "site 9" is located towards the C-terminus of the Greek key motif and contains GLY-86, ILE-88, PHE-94 and LYS-96. We also conducted an ultrahigh throughput *in silico* screen of commercially available compound libraries by generating a pseudo-ligand or "Exemplar" to identify compounds binding to site 2 in recombinant α-Syn fibrils.[18] We confirmed that the exemplar[19] method for screening large compound libraries is an effective method for identifying novel compounds that bind to α-Syn.

Since site 2 contains TYR-39, a site that is phosphorylated in α-Syn in PD brain,[20,21] we employed a similar strategy on a different compound library by using the exemplar generated from the prior work[18] for site 9, which does not contain any amino acid residues that undergo post-translational modification in PD brain.[22,23] This strategy resulted in the identification of a new ligand, **M503-1619**, which binds to α-Syn with high affinity and has low off-target binding to Aβ and tau. In this report, we describe the *in vitro* characterization of **[^{3}H]M503-1619** in postmortem samples of PD brain, and the radiosynthesis and *in vivo* evaluation of **[^{11}C]M503-1619** in PET imaging studies in non-human primates (NHPs). Our data suggest that **[^{11}C]M503-1619** is a promising lead compound for PET radiotracer for imaging α-Syn fibrils in PD.

2. Results and discussion

2.1. *In silico* ultrahigh throughput screening

A site 9 Exemplar generated from prior work[18] was used for the ultrahigh throughput *in silico* screening on a library of 42 million compounds. The top 3 million *in silico* hits were narrowed down to 40 000 compounds by using the secondary *in silico* filters, including pan-assay interference compounds (PAINS)[24] screening, central nervous system multiparameter optimization (CNS MPO)[25] scoring, and additional chemical properties filtering (*e.g.*, number of aromatic rings, molecular weight, and cLog*D*). Visual inspection led to identification of 6 compounds (compound **M503-1619**, **P035-0108**, **P706-0700**, **P706-0073**, **P706-0209**, and **P706-0701**) for further *in vitro* binding studies. The structures of the candidate ligands are shown in Table 1.

2.2. *In vitro* radioligand competition binding assays

For testing the binding affinity to α-Syn fibrils, competition binding assays were initially conducted in recombinant α-Syn fibrils using [^{3}H]BF-2846 as the radioligand. This radioligand was found to bind preferentially to site 9 in α-Syn fibrils.[17] **M503-1619**, **P706-0700** and **P706-0701** had a high affinity to α-Syn fibrils (K_i = 6.5 nM, 12.6 nM, and 12.1 nM *vs.* [^{3}H]BF-2846; Table 1). For determining their selectivity towards Aβ, the three ligands were further tested in AD brain tissue homogenates using [^{3}H]PiB as the competing radioligand. All the three ligands were found to have a low affinity to Aβ (K_i = 390 nM for **M503-1619** and $K_i > 1000$ for **P706-0700** and **P706-0701** *vs.* [^{3}H]PiB; Table 1).

Competition binding assays for tau were also conducted using several tritiated tau radioligands, including [^{3}H]MK-6240,[26] [^{3}H]PI-2620,[27] [^{3}H]Z-2340[28] and [^{3}H]CBD-2115,[29] in post-mortem samples of AD tissues (Table 2). [^{3}H]Chrysamine-G ([^{3}H]CG), which binds to a different site on Aβ than PiB,[30] was also included in this assay as an alternative measure of binding to Aβ (Table 2). The results of these studies revealed very low binding of **M503-1619** to tau and Aβ.

2.3. Chemistry

The route for the synthesis of **M503-1619** and its precursor **5** for radiolabeling studies with tritium and carbon-11 is shown in Scheme 1. Coupling the commercially available compound **1** and 1-(pyridin-2-yl)piperazine **2** using triethylamine (Et_3N) as base afforded intermediate **3** in moderate yield. Hydrolysis of the ester of **3** generated the carboxylic acid **4**. This acid coupled

Table 1 Results of *in vitro* competition binding assay for selected compounds

Compounds	Structure	α-Syn fibrils (K_i; nM)[a]	AD brain tissue homogenates (K_i; nM)[b]	CLogP	Molecular weight	Topological polar surface area
M503-1619	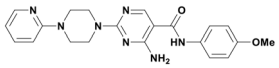	6.5 ± 2.9	390 ± 120	2.89	404.45	109.50
P035-0108	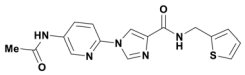	388.4 ± 178.9	>1000	2.00	341.39	117.15
P706-0700	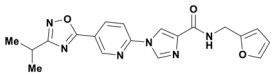	12.6 ± 1.0	>1000	2.32	378.38	111.87
P706-0073	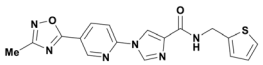	>1000	>1000	2.09	366.40	126.97
P706-0209	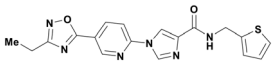	>1000	>1000	2.62	380.42	126.97
P706-0701	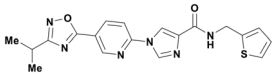	12.1 ± 2.9	>1000	3.02	394.45	126.97

[a] K_i values were determined from competitive radioligand binding full curves using recombinant α-Syn fibrils with [^{3}H]BF-2846. [b] K_i values were determined from competitive radioligand binding full curves using AD brain tissue homogenates with [^{3}H]PiB.

Table 2 Competition binding of **M503-1619** *vs.* different tritiated Aβ and tau radioligands in AD brain tissue homogenates

Radioligand	K_i (nM)
[^{3}H]CG	>10 000
[^{3}H]PI-2620	>10 000
[^{3}H]Z-2340	3700
[^{3}H]MK-6240	240
[^{3}H]CBD-2115	>10 000

with 4-methoxyaniline or 4-aminophenol delivered **M503-1619** and its precursor **5** in moderate yield.

2.4. *In vitro* saturation binding assays

To confirm the affinity and selectivity of **M503-1619** for α-Syn *versus* Aβ and tau, the corresponding tritiated compound was synthesized for direct binding assays. Saturation binding assays of [^{3}H]**M503-1619** in different human brain tissue homogenates (Table 3) confirmed the high binding affinity to synthetic α-Syn fibrils (K_d = 4.4 nM) and PD brain tissue homogenates (K_d = 2.5 nM). These results are consistent with the data from the competition binding assays. [^{3}H]**M503-1619** had a relatively low affinity for AD (K_d = 37 nM), progressive supranuclear palsy (PSP; K_d = 55 nM), and corticobasal degeneration (CBD; K_d = 94) tissues. The results of this study support the selectivity of this radioligand for α-Syn found in PD brain.

2.5. Autoradiography

A previous study from our lab demonstrated that the site 9 ligand, [^{3}H]HY-2-15 (Fig. 1) showed preferential binding α-Syn in postmortem brain sections of MSA and not PD.[31] An earlier study with a fluorescent probe displayed the opposite specificity, labeling α-Syn in Lewy bodies of PD brain and not the glial cytoplasmic inclusions (GCIs) in MSA brain.[32] Therefore, nuclear emulsion autoradiography of [^{3}H]**M503-1619** was performed on PD and MSA tissue sections to assess if it has specificity for the different forms of α-Syn (Fig. 2). High-resolution autoradiography visualized target engagement of [^{3}H]**M503-1619** to Lewy bodies in PD brain (Fig. 2A and B) but not

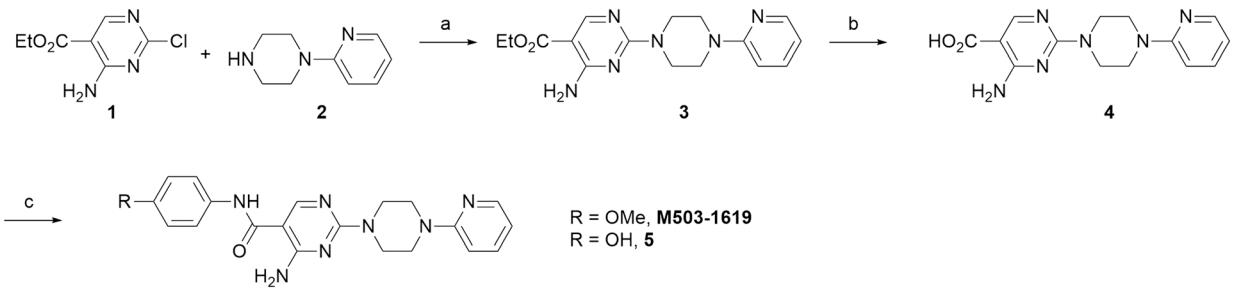

Scheme 1 Methods for preparing **M503-1619** and its precursor. Conditions: a) Et_3N, MeCN, rt., overnight; b) NaOH, EtOH, 50 °C, 4 h; c) 4-methoxyaniline or 4-aminophenol, HBTU, DIPEA, DMF, rt., overnight.

Table 3 Summary of saturation binding assays of [^{3}H]M503-1619 for various neurodegenerative diseases brain tissues

Tissue	K_d[a] (nM)	B_{max} (nM)
α-Syn fibrils (n = 4)	4.4 ± 1.0	1156 ± 112
PD (n = 4)	2.5 ± 0.3	59 ± 10
AD (n = 4)	37 ± 2	160 ± 28
PSP (n = 4)	55 ± 3	399 ± 24
CBD (n = 3)	94 ± 13	540 ± 130

[a] The K_d values are expressed as the mean ± SD by three individual experiments, all assays were performed in triplicate.

to GCIs present in MSA (Fig. 2C and D). α-Syn neuropathology visualized using anti-pS129 α-Syn immunohistochemistry (IHC) and high-resolution autoradiography with **[^{3}H]M503-1619** on the same section showed a clear overlap in the PD brain but not in the MSA (Fig. 2E–H). These data suggest that **[^{3}H]M503-1619** may be capable of differentiating α-Syn in PD *versus* MSA.

To further confirm these results from nuclear emulsion autoradiography, autoradiography studies (Fig. 3) were conducted in tissue sections from PD (hippocampus) and MSA (basal ganglia) cases. These images clearly showed a higher binding of the radioligand **[^{3}H]M503-1619** in PD (Fig. 3A) than in MSA (Fig. 3E), even though both brain specimens have a high burden of α-Syn measured with the antibody labeling conditions described above (Fig. 3B–D, and F–H). These results are consistent with the nuclear emulsion autoradiography and suggest that **[^{3}H]M503-1619** binds preferentially to α-Syn in PD and not MSA.

2.6. Radiosynthesis and PET imaging studies in NHPs

NHP PET imaging studies were conducted with **[^{11}C]M503-1619** to determine the brain uptake and rate of washout of the radiotracer from brain. **[^{11}C]M503-1619** was synthesized *via O*-alkylation of the phenol group of **5** with $^{11}CH_3I$ (Scheme 2).

The radiosynthesis required ~30 min to complete and **[^{11}C]M503-1619** was prepared in radiochemical yield of 56–63% (decay corrected to end of bombardment (EOB)) and a molar activity of ~1187 GBq μmol^{-1} (decay corrected to EOB).

PET imaging studies were conducted in two different species of NHPs, rhesus macaque and cynomolgus macaque. A total-body PET imaging study was conducted in a rhesus macaque on the PennPET Explorer[33] scanner at the University of Pennsylvania (Fig. 4), and a brain imaging study in a cynomolgus macaque was conducted on a Siemens Focus 220 system at Washington University in St. Louis (Fig. S1†). The PET images with **[^{11}C]M503-1619** showed high initial brain uptake. The peak uptake of the whole brain occurred at 2–3 min with a standardized uptake value (SUV) of 2.5 in rhesus monkey (Fig. 4) and 2.3 in cynomolgus monkey (Fig. S1†). Meanwhile, there was a rapid washout of **[^{11}C]M503-1619** from brain. The whole brain peak to 60 min ratio was 3.2 in both rhesus and cynomolgus monkeys. These study results demonstrated that the high initial brain uptake of **[^{11}C]M503-1619** and rapid washout makes it a suitable candidate for further *in vivo* PET image studies. Venous blood samples were analyzed for metabolites, which largely consisted of polar metabolites (Fig. S2 and Table S1†). **[^{11}C]M503-1619** was rapidly metabolized, with a parent fraction of 57% by 7.5 minutes post-injection, presenting a potential limitation to long duration scans and image quantification using blood-input based pharmacokinetic modeling.

3. Conclusions

[^{11}C]M503-1619 has a high affinity for α-Syn, moderate affinity for Aβ, and 10–20-fold selectivity *vs.* tau. Autoradiography studies

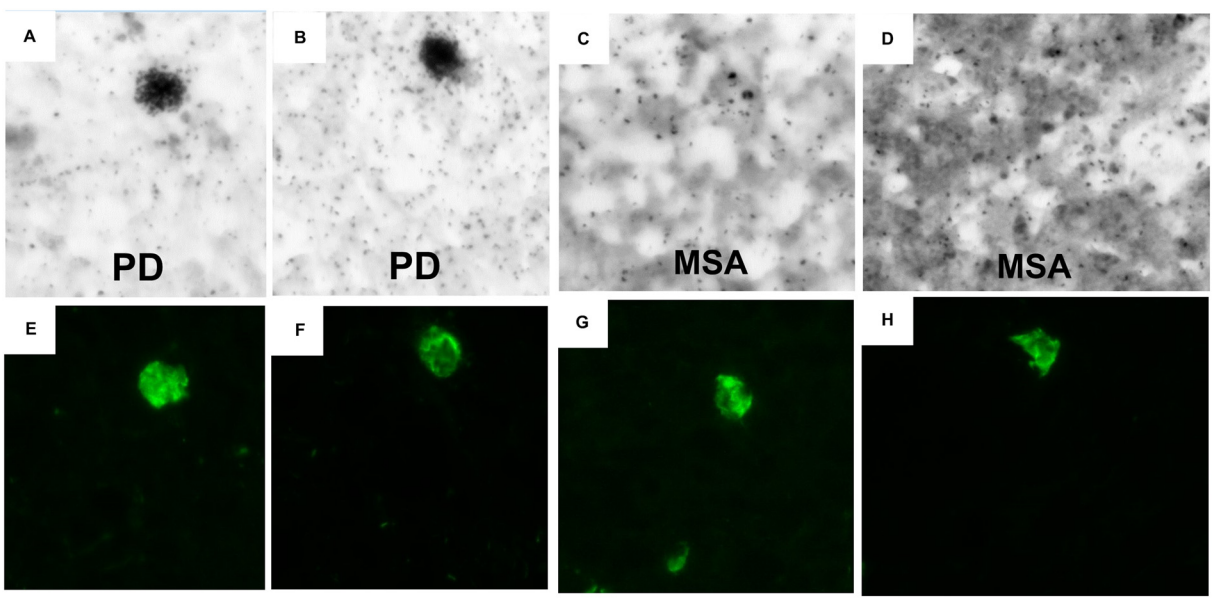

Fig. 2 High-resolution autoradiography with **[^{3}H]M503-1619** in PD (A) 5 nM, (B) 15 nM, and MSA brain tissue sections (C) 5 nM, (D) 15 nM, revealing accumulation of silver grains on Lewy bodies in PD but not on GCIs in MSA brain. Immunofluorescence with α-Syn–pS129 antibody in brain tissue sections from PD (E) and (F) and MSA (G) and (H) cases confirming α-Syn pathology.

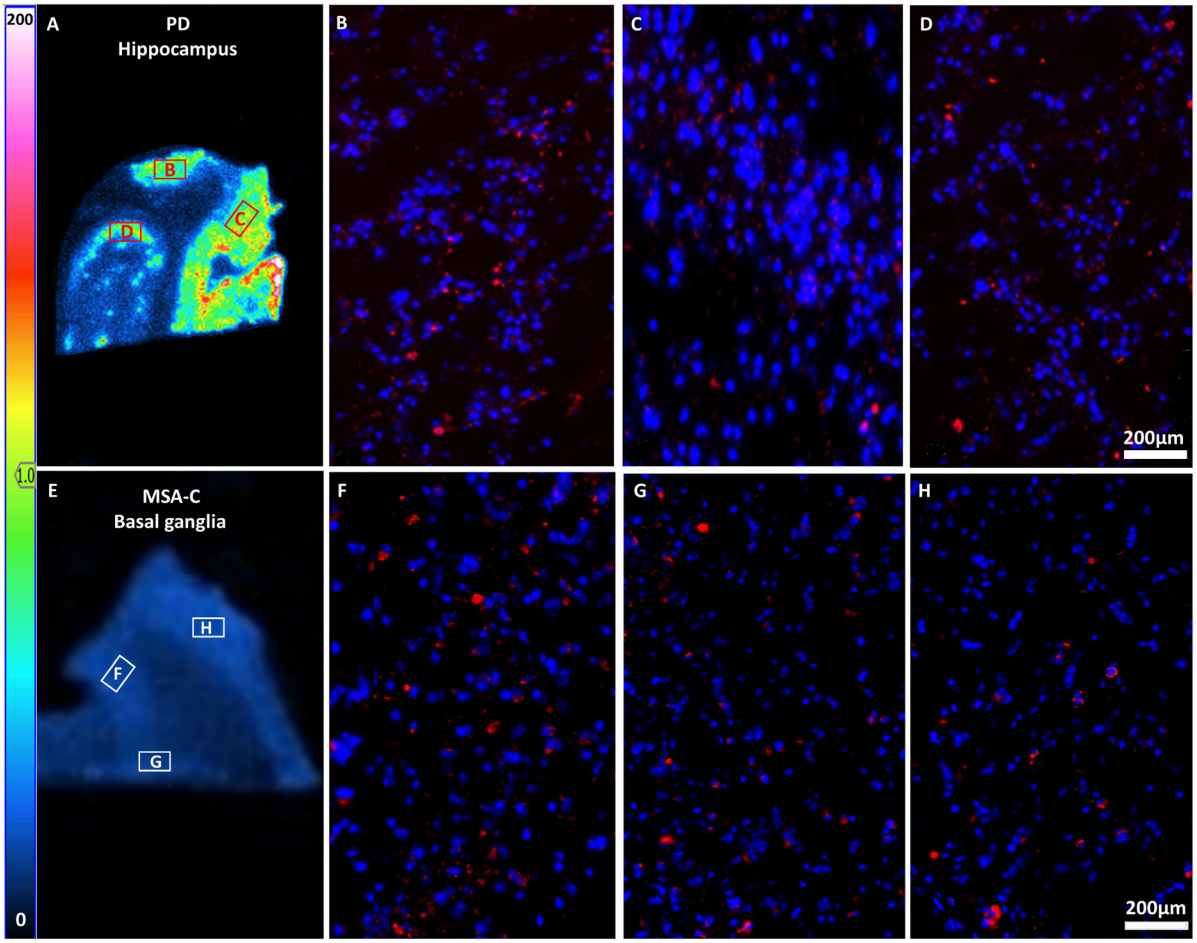

Fig. 3 Autoradiographic detection of [^{3}H]**M503-1619** binding (5 nM) in fresh–frozen postmortem brain tissue sections from (A) PD (hippocampus) and (E) MSA (basal ganglia) cases. Autoradiography color/brightness threshold levels are expressed in counts (0–200). (B–D) and (F–H) representative images of adjacent sections immunostained using pS129–α-synuclein antibody (red), and DAPI nuclear stain (blue) in areas indicated by squares in PD (A) and MSA (E) cases. Scale bar, 200 μm.

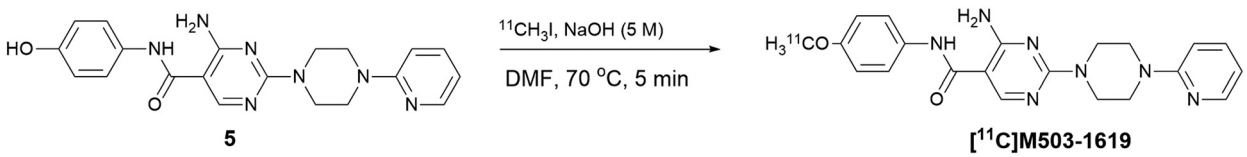

Scheme 2 The procedure for radiosynthesis of [^{11}C]**M503-1619**. Conditions: $^{11}CH_3I$, 5 M NaOH, DMF, 70 °C, 5 min.

suggest that it binds α-Syn in PD more robustly than in the MSA brain. The radiotracer has high brain uptake and rapid washout from the macaque brain. Our data suggest that **M503-1619** has suitable properties as a lead compound for a PET radiotracer development. Additional structure–activity relationship studies are ongoing with **M503-1619** to identify a suitable compound for translational imaging studies in PD patients.

4. Experimental

4.1. *In silico* compound screen

The 42 million compound database from Mcule, Inc. was used for the initial screen against the site 9 exemplar that was generated from our prior work.[18] The *in silico* conformers generation for compound library and the ultrahigh throughput screening were performed on the high-performance computing cluster at the Center for Biomedical Image Computing and Analytics at the University of Pennsylvania. Three-dimensional conformations of the compound database were generated using OMEGA (OpenEye Scientific Software, Inc.). Molecular alignment was performed using ROCS (OpenEye Scientific Software, Inc.). The top 3 million compounds as quantified by the sum Tanimoto coefficient of shape and pharmacophore similarities were retained for the secondary *in silico* screening. Compounds consisting of PAINS motifs, CNS MPO score lower than 4, number of aromatic ring lower than 2 or higher than 5,

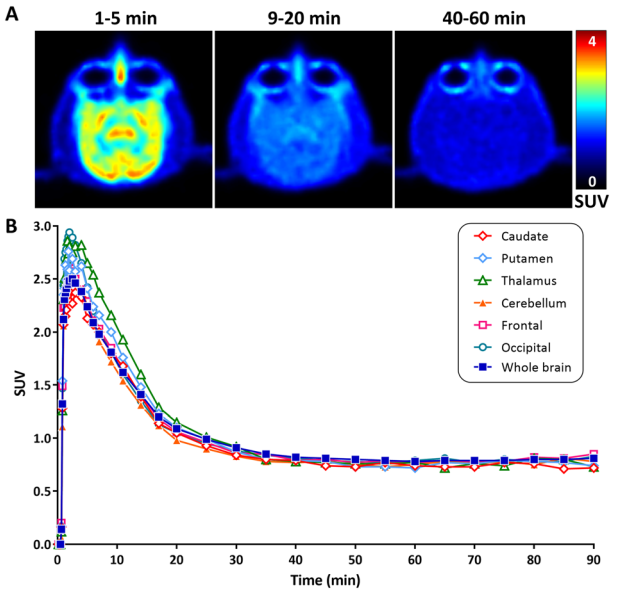

Fig. 4 *In vivo* PET study of the rhesus macaque for [^{11}C]**M503-1619**. (A) The representative brain images of 1–5 min, 9–20 min, and 40–60 min. (B) Time activity curves (TACs) of different brain regions for [^{11}C]**M503-1619**.

molecular weight higher than 500, and cLog*D* lower than 1 or higher than 3.5 were excluded from the initial *in silico* hits for the final visual inspection. Visual inspection was performed by two experienced chemists, and compounds were selected based on the linearity of the structure, the number of aromatic rings, and the presence and position of nitrogen atoms (*i.e.*, heteroaromatic rings) and substituents on the aromatic rings that could facilitate radiolabeling.

4.2. General

Commercial reagents and solvents were purchased from sources, including Sigma-Aldrich (MO, U.S.A.), Synthonix (NC, U.S.A.), Enamine (Kyiv, UA), Ambeed (IL, U.S.A), COMBI-BLOCKS (CA, U.S.A) or Thermo Fisher Scientific (MA, U.S.A.), and used as received. Thin layer chromatography (TLC) was performed using TLC silica gel 60 W F254S plates for monitoring reactions, and the spots were visualized under UV light (254 nm). Flash chromatography purifications were conducted on a Biotage Isolera One system (Uppsala, Sweden). ^{1}H and ^{13}C NMR spectra were recorded on a Bruker NEO-400 spectrometer (Bruker, MA, U.S.A.) with chemical shifts (δ) reported in parts per million (ppm) relative to the deuterated solvent as an internal reference. Mass spectra (m/z) were acquired on a 2695 Alliance LC-MS (Waters Corporation, MA, U.S.A.) with positive electrospray ionization (ESI), and high-resolution mass spectra (HRMS, m/z) were obtained using a waters LCT premier mass spectrometer (Waters Corporation, MA, U.S.A.). Recombinant α-Syn fibrils preparation including α-Syn protein expression and purification was performed according to the literature.[32] The synthesis of [^{3}H]**M503-1619** is provided in the ESI† and was conducted by Novandi Chemistry AB (Södertälje, Sweden).

4.3. Chemistry: the procedure for the synthesis of M503-1619 and its precursor 5

Ethyl 4-amino-2-(4-(pyridin-2-yl)piperazin-1-yl)pyrimidine-5-carboxylate (3). A solution of ethyl 4-amino-2-chloropyrimidine-5-carboxylate **1** (120 mg, 0.6 mmol) and 1-(pyridin-2-yl) piperazine **2** (147 mg, 0.9 mmol) in 15 mL dry MeCN was added to Et_3N (182 mg, 1.8 mmol). The mixture was stirred at room temperature overnight. The solvents were removed, and the crude product was purified by flash column chromatography on silica gel, eluting with hexanes/ethyl acetate (with 5% 7 N NH_3 in MeOH) (4 : 1 to 1 : 1) to afford the desired product **3** as a white solid. **^{1}H NMR (400 MHz, DMSO-d_6)** δ 8.52 (s, 1H), 8.12 (ddd, J = 4.9, 2.0, 0.8 Hz, 1H), 7.55 (ddd, J = 8.9, 7.1, 2.0 Hz, 1H), 7.47 (s, 1H), 7.41 (s, 1H), 6.86 (d, J = 8.6 Hz, 1H), 6.66 (dd, J = 6.7, 4.5 Hz, 1H), 4.21 (q, J = 7.1 Hz, 2H), 1.26 (t, J = 7.1 Hz, 3H); **^{13}C NMR (101 MHz, DMSO-d_6)** δ 166.1, 162.9, 161.5, 160.6, 158.9, 147.7, 137.8, 113.4, 107.4, 95.1, 59.9, 44.5, 43.0, 14.4. **LCMS**: 329 [M + H]$^{+}$; **HRMS** (ESI) calculated for $C_{16}H_{21}N_6O_2^{+}$ ([M + H^{+}]) 329.1721, found: 329.1745. White solid, 100 mg, 51%.

4-Amino-*N*-(4-methoxyphenyl)-2-(4-(pyridin-2-yl)piperazin-1-yl)pyrimidine-5-carboxamide (M503-1619) and its precursor (5). A suspension of compound **3** (65 mg, 0.2 mmol) and NaOH (40 mg) in EtOH and H_2O (2 mL/2 mL) was heated to 60 °C for 4 h. After cooling to room temperature, EtOH was removed under reduced pressure. 1 N HCl was used to make the solution pH = 7. The precipitated solid was filtered out and dried under high vacuum for 12 h. The crude product **4** was used for the next step without further purification.

A solution of the crude product **4**, DIPEA (77 mg, 0.6 mmol), and HBTU (80 mg, 0.21 mmol) in 4 mL DMF was stirred for 15 min at room temperature. Either 4-methoxyaniline (26 mg, 0.21 mmol) or 4-aminophenol (23 mg, 0.21 mmol) was added to the solution. The mixture was stirred at room temperature overnight, washed with 1 N $NaHCO_3$ solution extracted with DCM (3 × 25 mL), and dried over Na_2SO_4. The solvents were removed, and the residue was purified by flash column chromatography on silica gel, eluting with DCM/7 N NH_3 in MeOH = 95 : 5 to afford **M503-1619** or its precursor **5** as white solids.[34]

4-Amino-*N*-(4-methoxyphenyl)-2-(4-(pyridin-2-yl)piperazin-1-yl)pyrimidine-5-carboxamide (M503-1619). ^{1}H NMR (400 MHz, DMSO-d_6) δ 9.75 (s, 1H), 8.61 (s, 1H), 8.13 (d, J = 4.7 Hz, 1H), 7.64–7.45 (m, 4H), 6.95–6.85 (m, 3H), 6.66 (t, J = 5.9 Hz, 1H), 3.87 (t, J = 5.2 Hz, 4H), 3.73 (t, J = 1.5 Hz, 3H), 3.56 (t, J = 5.2 Hz, 4H); **^{13}C NMR (101 MHz, DMSO-d_6)** δ 165.4, 162.9, 160.9, 158.9, 157.4, 155.4, 147.6, 137.6, 132.0, 122.3, 113.7, 113.2, 107.2, 99.0, 55.2, 44.5, 42.9. **LCMS**: 406 [M + H]$^{+}$; **HRMS** (ESI) calculated for $C_{21}H_{24}N_7O_2^{+}$ ([M + H^{+}]) 406.1986, found: 406.1992. White solid, 35 mg, 43%.

4-Amino-*N*-(4-hydroxyphenyl)-2-(4-(pyridin-2-yl)piperazin-1-yl)pyrimidine-5-carboxamide (5). ^{1}H NMR (400 MHz, DMSO-d_6) δ 9.66 (s, 1H), 9.22 (s, 1H), 8.59 (s, 1H), 8.13 (ddd, J = 5.0, 2.0, 0.8 Hz, 1H), 7.56 (ddd, J = 8.9, 7.1, 2.0 Hz, 1H), 7.39 (d, J = 8.9 Hz, 2H), 6.87 (d, J = 8.6 Hz, 1H), 6.71 (d, J = 8.9 Hz, 2H), 6.66 (ddd, J = 7.2, 4.8, 0.8 Hz, 1H), 3.89–3.83 (m, 4H), 3.59–

3.52 (m, 4H); **^{13}C NMR (101 MHz, DMSO-d_6)** δ 165.2, 162.9, 160.9, 158.9, 157.3, 153.5, 147.6, 137.6, 130.5, 122.6, 114.9, 113.2, 107.3, 99.1, 44.5, 42.9. **LCMS**: 392 $[M + H]^+$. **HRMS** (ESI) calculated for $C_{20}H_{22}N_7O_2^+$ ($[M + H^+]$) 392.1829, found: 392.1836. White solid, 41 mg, 53%.

4.4. *In vitro* radioligand binding assays

Postmortem tissue. Post-mortem human brain tissues were collected by brain banks at the University of California, San Francisco (UCSF) and Banner/Sun Health AZ following informed consent of the donors and utilized at the University of Pittsburgh under the approval of the Committee for Oversight of Research and Clinical Training Involving Decedents (CORID no. 295). The binding assays utilized fresh frozen, autopsy-confirmed, post-mortem human AD, PSP, and CBD brain tissue blocks (1 cm^3) obtained from the Neurodegenerative Disease Brain Bank at UCSF, containing only frequent mixed 3R/4R-tau neurofibrillary tangles and Aβ plaque aggregates (AD tissue middle frontal gyrus), or only 4R-tau aggregates (PSP tissue, superior frontal gyrus, or CBD tissue, middle frontal gyrus) and no other detectable aggregated amyloid or TDP-43 species. Fresh frozen, autopsy-confirmed human PD anterior cingulate cortex brain tissue blocks (1 cm^3) were obtained from Dr. Thomas Beach at Banner Sun Health Research Institute, Sun City, AZ through the Michael J. Fox Foundation and contained frequent α-Syn aggregates and no other detectable aggregated amyloid or TDP-43 species. The frozen tissue blocks were separately thawed and homogenized in ice-cold pH 7.0 phosphate-buffered saline (PBS) at 300 mg mL^{-1} on ice using a glass homogenizer, diluted 30-fold with PBS to 10 mg mL^{-1} and homogenized a second time with a Brinkmann polytron homogenizer before storage at −80 °C. At the time of binding assays, frozen brain tissue homogenates were thawed to room temperature and diluted 10-fold in PBS to a concentration of 1 mg mL^{-1}. For Aβ assay, an AD brain sample was provided by the Penn Brain Bank and removed of most of the white matter before weighing the tissue. AD brain homogenates were prepared and stored at −80 °C before each binding assay.[35] The human PD tissue sample used in the homogenate binding assays was provided by Dr. Thomas Beach of the Banner Sun Health Research Institute, Sun City, AZ.

***In vitro* competition assays.** The equilibrium inhibition constant (K_i) values of the unlabeled compounds were determined *versus* tritium-labeled radioligands using published methods.[35] For the Mcule compounds, the 10 mM stock solutions in DMSO were diluted to the appropriate concentrations (ranging from 0.1 to 1000 nM) of unlabeled competitor in 400 μL of PBS buffer and combined with 500 μL of the tritium-labeled radioligand in PBS (~1 nM final concentration of radioligand). The assay was initiated by the addition of 100 μL of 1 mg mL^{-1} brain tissue homogenate to achieve a final concentration of 100 μg tissue per mL. After incubation for 60 min at room temperature, the binding mixture was filtered through a Whatman GF/B glass filter *via* a Brandel M-24R cell harvester (Gaithersburg, MD, USA) and rapidly washed four times with 3 mL of PBS buffer. The filters were counted in CytoScint-ES after thorough vortexing by using a liquid scintillation counter. Complete (100%) inhibition of specific binding was defined as the number of counts displaced by 1 μM unlabelled radioligand. All assays were performed in triplicate at each concentration.

Direct binding assays. [^{3}H]M503-1619 radioligand binding assays utilized AD, PSP, CBD, or PD brain homogenates to determine equilibrium dissociation constant (K_D) values and were performed with minor modifications of the procedure previously described in detail.[36] The unlabelled test compound was dissolved in DMSO at 400 μM and then diluted to 20 μM with PBS to yield 5% DMSO/PBS. The remaining serial dilutions (typically from 6 μM to 4 nM) were made with 5% DMSO/PBS to maintain a constant DMSO concentration in the final assay. Fifty μL of these solutions was combined with 50 μL of tritiated test compound and 800 μL of PBS to yield 0.25% DMSO, ~1 nM tritiated compound, and 0.2–1000 nM unlabelled compound in the final assay. The assay began by addition of 100 μL of the 1 mg mL^{-1} brain homogenate to achieve a final concentration of 100 μg tissue per mL. After incubation for 60 min at room temperature, the binding mixture was filtered through a Whatman GF/B glass filter *via* a Brandel M-24R cell harvester (Gaithersburg, MD) and rapidly washed three times with 3 mL of PBS. The filters were counted in CytoScint-ES after thorough vortexing and sitting overnight. All assays were performed at least in triplicate. The concentration of bound compound was determined from the radioactivity retained on the filter after correcting for the nondisplaceable radioactivity (defined as that remaining with ~1 μM unlabeled compound) and the specific activity of the tritiated compound after dilution with varying concentrations of unlabelled compound. The K_D value was determined by the slope (slope = $-1/K_D$) of a Scatchard plot of the bound/free *versus* bound radioligand values at the different ligand concentrations and the B_{max} value was determined by the *x*-axis intercept of the bound/free *versus* bound line.

4.5. *In vitro* real-time autoradiography

In vitro autoradiography was performed using 10 μm-thick fresh frozen sections derived from PD and MSA brains. Brain sections were first equilibrated for 30 min in 1× PBS (Dulbecco's phosphate buffered saline) and then incubated for 90 min at room temperature with 5 nM of **[^{3}H]M503-1619**. The sections were rinsed two times in cold buffer 1× (PBS + 20% EtOH) for 5 minutes, followed by a quick dip in cold distillated water. Non-specific binding was determined using 1 μM unlabeled **M503-1619**. Slides were then allowed to air-dry before being exposed and scanned in a real-time autoradiography system (BeaQuant instrument, ai4R, Nantes, France) for 2 h. ROI delineation and quantification of signal were performed using image analysis software, Beamage ai4R. Specific binding was determined by subtracting the non-

specific signal (NSB) from the total signal and expressed as counts min^{-1} mm^{-2}. Immunohistochemistry was performed on sections adjacent to those used for autoradiography. Sections were fixed in ethanol for 15 min, washed 3 × 5 min in PBS Tween-20 buffer, permeabilized with 0.1% Triton X-100 for 10 min. Sections underwent hydrogen peroxide blocking for 15 min and PBS + 10% goat serum + 1% BSA + 0.1% Tween 20 blocking for 1 h at room temperature. Sections were immunostained using primary antibody alpha synuclein (phospho S129) antibody (p-Syn/81A), used at 1 : 500 dilution overnight at 4 °C. After a series of thorough washes with PBS Tween 20 buffer, the slides were incubated with the secondary antibodies, Alexa Fluor 488at 1 : 1000 dilution for 1 h at RT. Subsequently, sections were mounted with Duolink *in situ* mounting media with DAPI and coverslips for microscopy. Images were captured with a Zeiss microscope at 10× magnification.

4.6. Nuclear emulsion autoradiography

Frozen postmortem PD and MSA brain tissue samples were sectioned on a cryostat at 16 μm and mounted onto glass slides and stored at −80 °C. To quench lipofuscin autofluorescence, slides were incubated in 1× TrueBlack (Biotium) in 70% EtOH. Slides were incubated sequentially with anti-phospho–α-Syn (S129) antibody (p-Syn/81A, BioLegend) and Alexa Fluor 488 goat anti-mouse secondary antibody to immunostain LBs and LNs. Slides were then incubated in 5 nM or 15 nM of **[^{3}H]M503-1619** diluted in 30 mM Tris–HCl, pH 7.4 for 2 h at 37 °C. The slides were washed in 30 mM Tris–HCl, pH 7.4 for 1 min, 50% ethanol/30 mM Tris–HCl, pH 7.4 for 1 min, 30% ethanol/30 mM Tris–HCl, pH 7.4 for 1 min, 30 mM Tris–HCl, pH 7.4 for 1 min, and MQH2O for 1 s. The slides were allowed to completely air dry in a fume hood. To obtain high resolution autoradiographic information, the slides were dipped in autoradiography emulsion (Carestream Type NTB) and incubated in the dark for 4 days. The slides were developed in Ilford Phenisol Developer for 4 min, 200 mL of 1% acetic acid for 2 min, 200 mL of 1 : 4 Ilford Hypam Fixer for 4 min, and 200 mL of MQH_2O for 4 min (2×). The slides were allowed to completely air dry in the fume hood before a coverslip was applied with Fluoromount-G mounting medium. Photomicrographs of fluorescent antibody staining and tritium activated silver grains were obtained on a Nikon Eclipse TE2000-U Inverted Fluorescence Microscope (Nikon, Tokyo, Japan) microscope using fluorescence and brightfield/monochrome light, respectively.

4.7. Radiosynthesis of [^{11}C]M503-1619

The radiolabeling of **[^{11}C]M503-1619** was performed using an automated synthesizer, Synthra MeIPlus (Synthra GmbH, Germany). The precursor **5** (1 mg, 2.5 μmol) was dissolved in 400 μL anhydrous DMF and 3 μL of 5 M NaOH solution. Radioactive [^{11}C]CH_3I gas was bubbled into the solution within 2–4 minutes. Then the reaction vial was sealed and heated at 70 °C for 5 minutes with stirring. The reaction was quenched with 1.3 mL of HPLC mobile phase (acetonitrile/ammonium formate solution 51/49 (v/v), pH = ∼4.5); and then loaded onto a semi-preparative HPLC system equipped with a C18 column (Agilent C18 column, 250 × 9.6 mm, 5 μM) and purified with a mobile phase flow rate of 4.0 mL min^{-1}. A UV detector set for a wavelength of 254 nm permitted purification. The target radioactive product was collected from 7 to 8 minutes using a glass vial prefilled with 50 mL Milli-Q water, then the solution was passed through a C-18 Sep-Pak cartridge (Part No. WAT020515, Waters Corporation, Milford, MA). After using 15 mL of Milli-Q water to rinse the C-18 cartridge, the radioactive product was eluted into a dose vial using 0.6 mL anhydrous ethanol, followed by diluting with 5.4 mL of saline to formulate the injection dose solution for administration to an animal.

An aliquot of the dose sample (20 μL) was injected into the analytic HPLC system for authentication by co-injection with the cold standard compound **M503-1619**, the chemical and radiochemical purity, and molar activity of the final dose were determined. The analytic HPLC system for quality control consists of a reversed-phase HPLC analytical column (Agilent Zorbax SB-C18, 4.6 mm × 250), UV wavelength of 254 nm, mobile phase of acetonitrile/0.1 M ammonium formate buffer (v/v, 75/25, pH = 4.5) with a flow rate of 1.0 mL min^{-1}. Under this condition, **[^{11}C]M503-1619** has a retention time of T_R = 4.0 min, 56–63% radiochemical yield (decay corrected to EOB), >1187 GBq μmol^{-1} molar activity (decay corrected to EOB), >95% chemical purity and >99% radiochemical purity.

4.8. Radiometabolite study of [^{11}C]M503-1619

Venous blood samples were collected throughout the PET scans to measure the radiometabolite profile. Blood samples were centrifuged for 5 minutes at 3000*g* to separate plasma. Plasma samples were treated with acetonitrile at 1 : 1 by volume and centrifuged to recover deproteinated plasma supernatant. The supernatant was injected into an Agilent Infinity 1280 HPLC (Agilent Technologies, Santa Clara, CA) with a reverse-phase Agilent Zorbax XDB-C18 analytical HPLC column (4.6 mm × 150) and a mobile phase of 65% 0.1 M ammonium formate buffer and 35% acetonitrile at 1.2 mL min^{-1}. Parent and metabolite activity fractions were measured with an in-line Posi-RAM detector (LabLogic Systems, Chantilly, VA) based on retention times of **M503-1619** standards.

4.9. PET studies of [^{11}C]M503-1619 in NHPs

PennPET Explorer. The NHP study was performed under protocols approved by the University of Pennsylvania Institutional Animal Care and Use Committee (IACUC). Dynamic total-body PET of **[^{11}C]M503-1619** was conducted on a 26-year-old adult male rhesus macaque using the PennPET Explorer scanner at the University of Pennsylvania. The monkey, fasted for 12 h prior to the PET study, was initially anesthetized by intramuscular injection with ketamine (4 mg kg^{-1}) and

dexmedetomidine (0.05 mg kg^{-1}). The monkey was intubated, and anesthesia was maintained with 0.75–2% isoflurane/oxygen. A percutaneous catheter was placed for the tracer injection. A low dose CT scan was performed to confirm positioning and attenuation correction followed by 90 min dynamic PET images (12 × 10 s, 2 × 30 s, 4 × 60 s, 2 × 120 s, 3 × 180 s, and 14 × 300 s) acquired in list-mode after venous injection of 105 MBq of [^{11}C] **M503-1619**. The PET image was reconstructed using time-of-flight list-mode ordered subsets expectation maximization (OSEM, 25 subsets) reconstruction algorithm.[37] The PET/CT imaging data was analyzed by using PMOD software (version 3.7, PMOD Technologies Ltd., Zurich, Switzerland). Seven volumes of interest (VOIs) for brain including caudate, putamen, thalamus, frontal cortex, occipital cortex, cerebellum, and whole brain were manually delineated on a T1-weighted MR image. TACs were extracted from all the VOIs and expressed as SUV.

MicroPET Focus 220. The NHP brain PET study was conducted following the Guidelines for the Care and Use of Research Animals under a research protocol approved by the Washington University Institutional Animal Care and Use Committee (IACUC). The microPET imaging was performed using a microPET Focus-220 scanner (Siemens Microsystems, Knoxville, TN). A male cynomolgus macaque (*Macaca fascicularis*; 8.5 kg) was used in this study. The animal was initially anesthetized with ketamine (10–20 mg kg^{-1}) and maintained with 40% N_2O and 60% O_2 with 1.0–1.5% isoflurane inhalation throughout the microPET imaging sessions. A 20 gauge plastic catheter was inserted into a limb vein to permit hydration and injection of the radiotracer. Prior to each PET emission acquisition, a 10 min transmission was used to confirm the position of the brain on the scanner followed by a 45 min transmission scan for attenuation correction. After administration of ~350 MBq of radiotracer, a two-hour dynamic emission scan data was acquired using the following time frames: 3 × 1 min, 4 × 2 min, 3 × 3 min, and 20 × 5 min.

A filtered back projection method was used to reconstruct PET images (volume size: 12 × 128 × 95, voxel size: 1.898 × 1.898 × 0.796 mm^3 in the x, y, and z direction) with dead time, scatter, and attenuation correction. To quantify the total tracer uptake in the brain, dynamic PET images were co-registered to a standardized monkey MRI template using PMOD software 4.02 (PMOD technologies, Zürich, Switzerland). A whole brain VOI was applied to the co-registered PET image to obtain the brain TAC. The uptake of radioactivity was normalized to body weight and the injected dose to obtain a SUV.

Data availability

The solid state NMR structure and exemplar for site 9 in alpha synuclein have been published previously.[18] The molecular alignment was performed using ROCS from Open Eye Scientific Software, Inc. (Albuquerque, NM). The compound database used in the *in silico* screen was commercially available from Mcule, Inc. (**https://mcule.com/database/**).

Author contributions

Conceptualization: R. H. M. Funding acquisition: R. H. M. Investigation, data curation, formal analysis, methodology and software: G.-L. T., C.-J. H., D. S. G., T. J. A. G., Z. L.-Z., C. T., W. K. C, A. J. Y., J.-G. C., K. P., T. H., H. J, Y. Y., C. H., S. G., H. L. and J. O. Project administration: C. A. M. and R. H. M. Resource, supervision, and validation: E. J. P, P. K., Z. T., C. A. M. and R. H. M. Visualization: C.-J. H. and R. H. M. Writing – original draft: G.-L. T., C-J. H. and R. H. M. Writing – review & editing: E. J. P., P. K., Z. T., C. A. M. and R. H. M.

Conflicts of interest

There are no conflicts to declare.

Acknowledgements

The authors would like to thank Mr. Mark Schneider for his excellent technical assistance. This work was funded by NIH grant U19-NS110456. The *in silico* studies were conducted on the high-performance Biomedical Image Computing and Informatics Cluster at the University of Pennsylvania, Center for Biomedical Image Computing and Analytics supported by the National Institutes of Health. We thank the University of Pennsylvania Physics and Instrumentation Group for the assistance with PennPET Explorer imaging studies.

References

1 E. R. Dorsey, T. Sherer, M. S. Okun and B. R. Bloem, *J. Parkinson's Dis.*, 2018, **8**, S3–S8.

2 V. L. Feigin, A. A. Abajobir, K. H. Abate, F. Abd-Allah, A. M. Abdulle, S. F. Abera, G. Y. Abyu, M. B. Ahmed, A. N. Aichour, I. Aichour, M. T. E. Aichour, R. O. Akinyemi, S. Alabed, R. Al-Raddadi, N. Alvis-Guzman, A. T. Amare, H. Ansari, P. Anwari, J. Ärnlöv, H. Asayesh, S. W. Asgedom, T. M. Atey, L. Avila-Burgos, E. Frinel, G. A. Avokpaho, M. R. Azarpazhooh, A. Barac, M. Barboza, S. L. Barker-Collo, T. Bärnighausen, N. Bedi, E. Beghi, D. A. Bennett, I. M. Bensenor, A. Berhane, B. D. Betsu, S. Bhaumik, S. M. Birlik, S. Biryukov, D. J. Boneya, L. N. B. Bulto, H. Carabin, D. Casey, C. A. Castañeda-Orjuela, F. Catalá-López, H. Chen, A. A. Chitheer, R. Chowdhury, H. Christensen, L. Dandona, R. Dandona, G. A. de Veber, S. D. Dharmaratne, H. P. Do, K. Dokova, E. R. Dorsey, R. G. Ellenbogen, S. Eskandarieh, M. S. Farvid, S.-M. Fereshtehnejad, F. Fischer, K. J. Foreman, J. M. Geleijnse, R. F. Gillum, G. Giussani, E. M. Goldberg, P. N. Gona, A. C. Goulart, H. C. Gugnani, R. Gupta, V. Hachinski, R. Gupta, R. R. Hamadeh, M. Hambisa, G. J. Hankey, H. A. Hareri, R. Havmoeller, S. I. Hay, P. Heydarpour, P. J. Hotez, M. B. Jakovljevic, M. Javanbakht, P. Jeemon, J. B. Jonas, Y. Kalkonde, A. Kandel, A. Karch, A. Kasaeian, A. Kastor, P. N. Keiyoro, Y. S. Khader, I. A. Khalil, E. A. Khan, Y.-H. Khang, A. Tawfih, A. Khoja, J. Khubchandani, C. Kulkarni, D. Kim, Y. J. Kim, M. Kivimaki, Y. Kokubo, S. Kosen, M. Kravchenko, R. V. Krishnamurthi, B. Kuate Defo, G. A. Kumar, R. Kumar,

H. H. Kyu, A. Larsson, P. M. Lavados, Y. Li, X. Liang, M. L. Liben, W. D. Lo, G. Logroscino, P. A. Lotufo, C. T. Loy, M. T. Mackay, H. M. A. El Razek, M. M. A. El Razek, A. Majeed, R. Malekzadeh, T. Manhertz, L. G. Mantovani, J. Massano, M. Mazidi, C. McAlinden, S. Mehata, M. M. Mehndiratta, Z. A. Memish, W. Mendoza, M. A. Mengistie, G. A. Mensah, A. Meretoja, H. B. Mezgebe, T. R. Miller, S. R. Mishra, N. M. Ibrahim, A. Mohammadi, K. E. Mohammed, S. Mohammed, A. H. Mokdad, M. Moradi-Lakeh, I. M. Velasquez, K. I. Musa, M. Naghavi, J. W. Ngunjiri, C. T. Nguyen, G. Nguyen, Q. L. Nguyen, T. H. Nguyen, E. Nichols, D. N. A. Ningrum, V. M. Nong, B. Norrving, J. J. N. Noubiap, F. A. Ogbo, M. O. Owolabi, J. D. Pandian, P. G. Parmar, D. M. Pereira, M. Petzold, M. R. Phillips, M. A. Piradov, R. G. Poulton, F. Pourmalek, M. Qorbani, A. Rafay, M. Rahman, M. H. Rahman, R. K. Rai, S. Rajsic, A. Ranta, S. Rawaf, A. M. N. Renzaho, M. S. Rezai, G. A. Roth, G. Roshandel, E. Rubagotti, P. Sachdev, S. Safiri, R. Sahathevan, M. A. Sahraian, A. M. Samy, P. Santalucia, I. S. Santos, B. Sartorius, M. Satpathy, M. Sawhney, M. I. Saylan, S. G. Sepanlou, M. A. Shaikh, R. Shakir, M. Shamsizadeh, K. N. Sheth, M. Shigematsu, H. Shoman, D. A. S. Silva, M. Smith, E. Sobngwi, L. A. Sposato, J. D. Stanaway, D. J. Stein, T. J. Steiner, L. J. Stovner, R. S. Abdulkader, C. E. I. Szoeke, R. Tabarés-Seisdedos, D. Tanne, A. M. Theadom, A. G. Thrift, D. L. Tirschwell, R. Topor-Madry, B. X. Tran, T. Truelsen, K. B. Tuem, K. N. Ukwaja, O. A. Uthman, Y. Y. Varakin, T. Vasankari, N. Venketasubramanian, V. V. Vlassov, F. Wadilo, T. Wakayo, M. T. Wallin, E. Weiderpass, R. Westerman, T. Wijeratne, C. S. Wiysonge, M. A. Woldu, C. D. A. Wolfe, D. Xavier, G. Xu, Y. Yano, H. H. Yimam, N. Yonemoto, C. Yu, Z. Zaidi, M. E. S. Zaki, J. R. Zunt, C. J. L. Murray and T. Vos, *Lancet Neurol.*, 2017, **16**, 877–897.

3 M. Baba, S. Nakajo, P. H. Tu, T. Tomita, K. Nakaya, V. M. Lee, J. Q. Trojanowski and T. Iwatsubo, *Am. J. Pathol*, 1998, **152**, 879–884.

4 M. G. Spillantini, M. L. Schmidt, V. M. Lee, J. Q. Trojanowski, R. Jakes and M. Goedert, *Nature*, 1997, **388**, 839–840.

5 C. M. Clark, J. A. Schneider, B. J. Bedell, T. G. Beach, W. B. Bilker, M. A. Mintun, M. J. Pontecorvo, F. Hefti, A. P. Carpenter, M. L. Flitter, M. J. Krautkramer, H. F. Kung, R. E. Coleman, P. M. Doraiswamy, A. S. Fleisher, M. N. Sabbagh, C. H. Sadowsky, E. M. Reiman, S. P. Zehntner, D. M. Skovronsky and T. A.-A. S. Group, *JAMA, J. Am. Med. Assoc.*, 2011, **305**, 275–283.

6 W. E. Klunk, H. Engler, A. Nordberg, Y. Wang, G. Blomqvist, D. P. Holt, M. Bergström, I. Savitcheva, G.-F. Huang, S. Estrada, B. Ausén, M. L. Debnath, J. Barletta, J. C. Price, J. Sandell, B. J. Lopresti, A. Wall, P. Koivisto, G. Antoni, C. A. Mathis and B. Långström, *Ann. Neurol.*, 2004, **55**, 306–319.

7 C.-F. Xia, J. Arteaga, G. Chen, U. Gangadharmath, L. F. Gomez, D. Kasi, C. Lam, Q. Liang, C. Liu, V. P. Mocharla, F. Mu, A. Sinha, H. Su, A. K. Szardenings, J. C. Walsh, E. Wang, C. Yu, W. Zhang, T. Zhao and H. C. Kolb, *Alzheimer's Dementia*, 2013, **9**, 666–676.

8 J. L. Eberling, K. D. Dave and M. A. Frasier, *J. Parkinson's Dis.*, 2013, **3**, 565–567.

9 C. A. Mathis, B. J. Lopresti, M. D. Ikonomovic and W. E. Klunk, *Semin. Nucl. Med.*, 2017, **47**, 553–575.

10 D. P. Bagchi, L. Yu, J. S. Perlmutter, J. Xu, R. H. Mach, Z. Tu and P. T. Kotzbauer, *PLoS One*, 2013, **8**, e55031.

11 E. T. L'Estrade, M. Erlandsson, F. G. Edgar, T. Ohlsson, G. M. Knudsen and M. M. Herth, *Neuropharmacology*, 2020, **172**, 107830.

12 M. Shah, J. Seibyl, A. Cartier, R. Bhatt and A. M. Catafau, *J. Nucl. Med.*, 2014, **55**, 1397–1400.

13 R. Smith, F. Capotosti, M. Schain, T. Ohlsson, E. Vokali, J. Molette, T. Touilloux, V. Hliva, I. K. Dimitrakopoulos, A. Puschmann, J. Jögi, P. Svenningsson, M. Andréasson, C. Sandiego, D. S. Russell, P. Miranda-Azpiazu, C. Halldin, E. Stomrud, S. Hall, K. Bratteby, E. Tampio L'Estrade, R. Luthi-Carter, A. Pfeifer, M. Kosco-Vilbois, J. Streffer and O. Hansson, *Nat. Commun.*, 2023, **14**, 6750.

14 J. Xiang, Y. Tao, Y. Xia, S. Luo, Q. Zhao, B. Li, X. Zhang, Y. Sun, W. Xia, M. Zhang, S. S. Kang, E.-H. Ahn, X. Liu, F. Xie, Y. Guan, J. J. Yang, L. Bu, S. Wu, X. Wang, X. Cao, C. Liu, Z. Zhang, D. Li and K. Ye, *Cell*, 2023, **186**(3350–3367), e3319.

15 H. Wood, *Nat. Rev. Neurol.*, 2013, **9**, 599.

16 H. Endo, M. Ono, Y. Takado, K. Matsuoka, M. Takahashi, K. Tagai, Y. Kataoka, K. Hirata, K. Takahata, C. Seki, N. Kokubo, M. Fujinaga, W. Mori, Y. Nagai, K. Mimura, K. Kumata, T. Kikuchi, A. Shimozawa, S. K. Mishra, Y. Yamaguchi, H. Shimizu, A. Kakita, H. Takuwa, H. Shinotoh, H. Shimada, Y. Kimura, M. Ichise, T. Suhara, T. Minamimoto, N. Sahara, K. Kawamura, M.-R. Zhang, M. Hasegawa and M. Higuchi, *Neuron*, 2024, 599.

17 C. J. Hsieh, J. J. Ferrie, K. Xu, I. Lee, T. J. A. Graham, Z. Tu, J. Yu, D. Dhavale, P. Kotzbauer, E. J. Petersson and R. H. Mach, *ACS Chem. Neurosci.*, 2018, **9**, 2521–2527.

18 J. J. Ferrie, Z. Lengyel-Zhand, B. Janssen, M. G. Lougee, S. Giannakoulias, C. J. Hsieh, V. V. Pagar, C. C. Weng, H. Xu, T. J. A. Graham, V. M. Lee, R. H. Mach and E. J. Petersson, *Chem. Sci.*, 2020, **11**, 12746–12754.

19 D. K. Johnson and J. Karanicolas, *PLoS Comput. Biol.*, 2013, **9**, e1002951.

20 B. Sonustun, M. F. Altay, C. Strand, K. Ebanks, G. Hondhamuni, T. T. Warner, H. A. Lashuel and R. Bandopadhyay, *Cells*, 2022, **11**, 906.

21 K. Zhao, Y. J. Lim, Z. Liu, H. Long, Y. Sun, J. J. Hu, C. Zhao, Y. Tao, X. Zhang, D. Li, Y. M. Li and C. Liu, *Proc. Natl. Acad. Sci. U. S. A.*, 2020, **117**, 20305–20315.

22 S. X. Pancoe, Y. J. Wang, M. Shimogawa, R. M. Perez, S. Giannakoulias and E. J. Petersson, *J. Mol. Biol.*, 2022, **434**, 167859.

23 S. Zhang, R. Zhu, B. Pan, H. Xu, M. F. Olufemi, R. J. Gathagan, Y. Li, L. Zhang, J. Zhang, W. Xiang, E. M. Kagan, X. Cao, C. Yuan, S.-J. Kim, C. K. Williams, S. Magaki, H. V. Vinters, H. A. Lashuel, B. A. Garcia, E. J. Petersson, J. Q. Trojanowski, V. M.-Y. Lee and C. Peng, *Nat. Neurosci.*, 2023, **26**, 213–225.

24 J. B. Baell and G. A. Holloway, *J. Med. Chem.*, 2010, **53**, 2719–2740.

25 T. T. Wager, X. Hou, P. R. Verhoest and A. Villalobos, *ACS Chem. Neurosci.*, 2016, **7**, 767–775.
26 A. M. Walji, E. D. Hostetler, H. Selnick, Z. Zeng, P. Miller, I. Bennacef, C. Salinas, B. Connolly, L. Gantert, M. Holahan, S. O'Malley, M. Purcell, K. Riffel, J. Li, J. Balsells, J. A. OBrien, S. Melquist, A. Soriano, X. Zhang, A. Ogawa, S. Xu, E. Joshi, J. D. Rocca, F. J. Hess, J. Schachter, D. Hesk, D. Schenk, A. Struyk, K. Babaoglu, T. G. Lohith, Y. Wang, K. Yang, J. Fu, J. L. Evelhoch and P. J. Coleman, *J. Med. Chem.*, 2016, **59**, 4778–4789.
27 H. Kroth, F. Oden, J. Molette, H. Schieferstein, F. Capotosti, A. Mueller, M. Berndt, H. Schmitt-Willich, V. Darmency, E. Gabellieri, C. Boudou, T. Juergens, Y. Varisco, E. Vokali, D. T. Hickman, G. Tamagnan, A. Pfeifer, L. Dinkelborg, A. Muhs and A. Stephens, *Eur. J. Nucl. Med. Mol. Imaging*, 2019, **46**, 2178–2189.
28 T. J. Graham, A. Lindberg, J. Tong, J. S. Stehouwer, N. Vasdev, R. H. Mach and C. A. Mathis, *J. Med. Chem.*, 2023, **66**, 10628–10638.
29 A. Lindberg, A. C. Knight, D. Sohn, L. Rakos, J. Tong, A. Radelet, N. S. Mason, J. S. Stehouwer, B. J. Lopresti, W. E. Klunk, J. Sandell, A. Sandberg, P. Hammarström, S. Svensson, C. A. Mathis and N. Vasdev, *ACS Chem. Neurosci.*, 2021, **12**, 596–602.
30 C. A. Mathis, N. S. Mason, B. J. Lopresti and W. E. Klunk, *Semin. Nucl. Med.*, 2012, **42**, 423–432.
31 H. Y. Kim, W. K. Chia, C.-J. Hsieh, D. S. Guarino, T. J. Graham, Z. Lengyel-Zhand, M. Schneider, C. Tomita, M. G. Lougee, H. J. Kim, V. V. Pagar, H. Lee, C. Hou, B. A. Garcia, E. J. Petersson, J. O'Shea, P. T. Kotzbauer, C. A. Mathis, V. M.-Y. Lee, K. C. Luk and R. H. Mach, *J. Med. Chem.*, 2023, **66**, 12185–12202.
32 Z. Lengyel-Zhand, J. J. Ferrie, B. Janssen, C. J. Hsieh, T. Graham, K. Y. Xu, C. M. Haney, V. M. Lee, J. Q. Trojanowski, E. J. Petersson and R. H. Mach, *Chem. Commun.*, 2020, **56**, 3567–3570.
33 B. Dai, M. E. Daube-Witherspoon, S. McDonald, M. E. Werner, M. J. Parma, M. J. Geagan, V. Viswanath and J. S. Karp, *Phys. Med. Biol.*, 2023, **68**, 095007.
34 T. Ryckmans, A. A. Aubdool, J. V. Bodkin, P. Cox, S. D. Brain, T. Dupont, E. Fairman, Y. Hashizume, N. Ishii, T. Kato, L. Kitching, J. Newman, K. Omoto, D. Rawson and J. Strover, *Bioorg. Med. Chem. Lett.*, 2011, **21**, 4857–4859.
35 W. E. Klunk, Y. Wang, G. F. Huang, M. L. Debnath, D. P. Holt, L. Shao, R. L. Hamilton, M. D. Ikonomovic, S. T. DeKosky and C. A. Mathis, *J. Neurosci.*, 2003, **23**, 2086–2092.
36 W. E. Klunk, Y. Wang, G.-f. Huang, M. L. Debnath, D. P. Holt and C. A. Mathis, *Life Sci.*, 2001, **69**, 1471–1484.
37 A. R. Pantel, V. Viswanath, M. E. Daube-Witherspoon, J. G. Dubroff, G. Muehllehner, M. J. Parma, D. A. Pryma, E. K. Schubert, D. A. Mankoff and J. S. Karp, *J. Nucl. Med.*, 2020, **61**, 144–151.